AD-A187 456 MBE GROWTH CHARACTERIZATION AND ELECTRONIC DEVICE PROCESSING OF HGCDTE HG (U) ILLINOIS UNIV AT CHICAGO CIRCLE DEPT OF PHYSICS J FAURIE 15 MAR 87 1/1

UNCLASSIFIED AFOSR-TR-87-1628 F49620-87-C-0021 F/G 20/12 NL

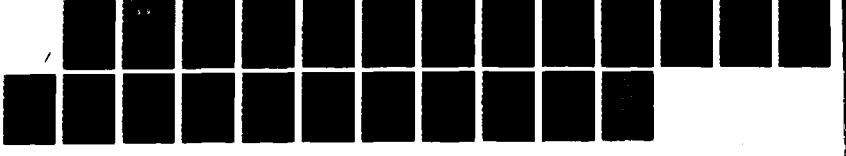

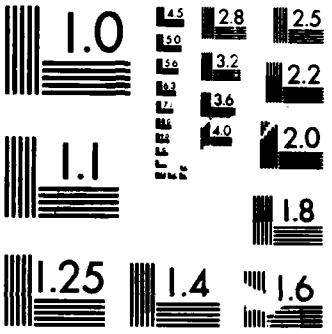

8a. NAME OF FUNDING/SPONSORING ORGANIZATION	8b. OFFICE SYMBOL (If applicable)	9. PROCUREMENT INSTRUMENT IDENTIFICATION NUMBER
AFOSR	NE	F49620-87-C-0021

8c. ADDRESS (City, State and ZIP Code)	10. SOURCE OF FUNDING NOS.			
	PROGRAM ELEMENT NO.	PROJECT NO.	TASK NO.	WORK UNIT NO.
Building 410 Bolling Air Force Base Washington, DC 20332-6448	61102F	DARPA		

11. TITLE (Include Security Classification) MBE GROWTH CHARACTERIZATION & ELECTRONIC DEVICE PROCESSING OF HgCdTe, HgZnTe, RELATED HETEROJUNCTIONS AND HgCdTe-CdTe SUPERLATTICES

12. PERSONAL AUTHOR(S) JEAN-PIERRE FAURIE

13a. TYPE OF REPORT	13b. TIME COVERED	14. DATE OF REPORT (Yr., Mo., Day)	15. PAGE COUNT
QUARTERLY	FROM 3/15/87 TO _____	87/03/15	21

16. SUPPLEMENTARY NOTATION

17. COSATI CODES			18. SUBJECT TERMS (Continue on reverse if necessary and identify by block number)
FIELD	GROUP	SUB. GR.	

19. ABSTRACT (Continue on reverse if necessary and identify by block number)

Results obtained for MBE grown N & P-type layers in terms of carrier concentration and electron or hole mobilities. Most layers grown after the start date of the current contract. It is important to point out that even if these results are the best ever obtained in the laboratory they are representative of our level of control concerning the growth. Numerous layers with the same composition exhibit very similar results. A new Hg cell, which is a prototype built by ISA - Riber is currently being tested in the laboratory. This cell that we have conceived gives a very stable Hg flux during hours of growth. It should be noted that both mobility and carrier concentration values are suitable for IR device application.

20. DISTRIBUTION/AVAILABILITY OF ABSTRACT	21. ABSTRACT SECURITY CLASSIFICATION
UNCLASSIFIED/UNLIMITED ☒ SAME AS RPT. ☐ DTIC USERS ☐	UNCLASSIFIED

22a. NAME OF RESPONSIBLE INDIVIDUAL	22b. TELEPHONE NUMBER (Include Area Code)	22c. OFFICE SYMBOL
Jean-Pierre Faurie Capt Kevin Malloy	(312) 996-3400 767-4931	NE

MBE GROWTH, CHARACTERIZATION AND ELECTRONIC DEVICE PROCESSING OF HgCdTe, HgZnTe, RELATED HETEROJUNCTIONS AND HgCdTe-CdTe SUPERLATTICES

DARPA - AFOSR - F49620-87-C-0021
November 13, 1986 - November 12, 1989

Quarterly Report
March 15, 1987

Jean-Pierre Faurie
University of Illinois at Chicago

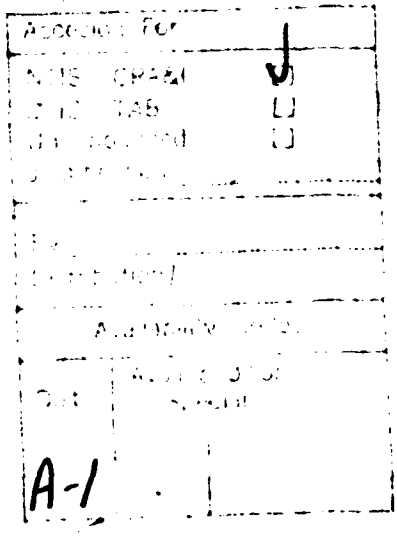

I. Growth and characterization of high quality HgCdTe

Table I and Table II illustrate the best results obtained for MBE grown N and P-type layers in terms of carrier concentration and electron or hole mobilities.

Most of these layers have been grown after the starting date of the current contract. An update of these data will be given when appropriate in order to follow the progress that the group is making during the contract. It is important to point out that even if these results are the best ever obtained in the laboratory they are representative of our level of control concerning the growth. Numerous layers with the same composition exhibit very similar results.

A new Hg cell, which is a prototype built by ISA - Riber is currently tested in the laboratory. This cell that we have conceived gives a very stable Hg flux during hours of growth. In table I and II it can be seen that thick layers can be grown using this cell (Sample # 131-318, 2-310, 19405 for example)

Electron mobilities are above 1×10^5 $cm^2V^{-1}s^{-1}$ what is expected for a high quality HgCdTe material with x of about 0.20.

Hole mobilities are very good in the 20% composition and excellent for layers grown on CdTeSe substrate (μh=840 $cm^2V^{-1}s^{-1}$ for x=0.31).

From our result it seems premature to draw a conclusion regarding the choice of the substrate. Electron or hole mobilities are very similar whatever the substrate used to grow HgCdTe.

Table III presents a comparison between (111)B and (100) orientation. Once again, the highest values obtained for electron mobilities are identical for both orientation. However, due to the twinning problem frequently observed in the (111)B, electron mobilities are in average lower for this orientation but, on the other hand, we have demonstrated that the (100) orientation required more mercury than the (111)B orientation.

Most of the layers reported in these tables have a carrier concentration N_a-N_d or N_d-N_a in the mid or low $10^{15}cm^{-3}$ range below 77K.

It should be noted that both mobility and carrier concentration values are suitable for IR device application.

ELECTRICAL CHARACTERISTICS OF HgCdTe MBE P-TYPE LAYERS GROWN BETWEEN 185-195°C. $(\bar{1}\bar{1}\bar{1})$B ORIENTATION

SAMPLE	SUBSTRATE	COMPOSITION X	THICKNESS e(μm)	T(K)	CARRIER CONCENTRATION $N_A-N_D(cm^{-3})$	MOBILITY $U_H(cm^2V^{-1}S^{-1})$
7434(1981)	CdTe	0.20	5.5	77	2×10^{15}	660
103 199	CdTe	0.25	8.8	40	2.6×10^{15}	550
128 311	CdTe	0.30	7.4	23	1.0×10^{15}	360
131 318	CdTe	0.33	12.3	40	1.7×10^{14}	240
507 321	GaAs	0.20	4.3	40	5.9×10^{15}	840
392 243	GaAs	0.22	1.5	40	2.2×10^{15}	520
393 244	GaAs	0.28	1.3	40	2.8×10^{15}	520
500 308	GaAs	0.31	2.3	30	1.1×10^{15}	450
1-309	CdTeSe	0.31	5.0	30	2.4×10^{15}	700
2-310	CdTeSe	0.32	9.4	30	1.2×10^{15}	670
4-319	CdTeSe	0.31	7.6	30	2.4×10^{15}	840

IMPORTANT : No HgTe layer at the interface

ELECTRICAL CHARACTERISTICS OF HgCdTe MBE N-TYPE LAYERS GROWN BETWEEN 180-190°C x ~ 0.2

SAMPLE	SUBSTRATE	ORIENTATION	COMPOSITION X	THICKNESS e(μm)	T	CARRIER CONCENTRATION $N_D-N_A(cm^{13})$	MOBILITY $U_H(cm^2V^{-1}s^{-1})$
7233	CdTe (1981)	(111)B	0.20	6.0μm	77K	2×10^{15}	1.9×10^5
11570	CdTe	(111)B	0.20	5.0μm	77K	1×10^{16}	1.2×10^5
19405	CdZnTe	(111)B	0.20	9.0μm	77K	2×10^{15}	1.2×10^5
576396	GaAs	(111)B	0.18	2.7μm	30K	1.5×10^{15}	5.0×10^5
283163	GaAs	(111)B	0.20	2.0μm	20K	7×10^{14}	1.2×10^5
191102	GaAs	(111)B	0.22	1.0μm	50K	4×10^{15}	1.0×10^5

ELECTRICAL CHARACTERISTICS OF HgCdTe MBE N-TYPE LAYERS GROWN BETWEEN 180-190°C x ~ 0.2

SAMPLE	SUBSTRATE	ORIENTATION	COMPOSITION X	THICKNESS e(μm)	T	CARRIER CONCENTRATION $N_D-N_A(cm^{13})$	MOBILITY $U_H(cm^2V^{-1}s^{-1})$
191102	GaAs	(111)B	0.22	1.0μm	50K	4×10^{15}	1.0×10^5
11570	CdTe	(111)B	0.20	5.0μm	77K	1×10^{16}	1.2×10^5
283163	GaAs	(111)B	0.20	2.0μm	20K	7×10^{14}	1.2×10^5
7233(1981)	CdTe	(111)B	0.2	6.0μm	77K	2×10^{15}	1.9×10^5
576396	GaAs	(111)B	0.18	2.7μm	30K	1.5×10^{15}	5.0×10^5
11871	CdTe	(100)	0.20	5.0μm	77K	2×10^{16}	1.4×10^5
162431	CdTe	(100)	0.22	2.0μm	77K	6.0×10^{15}	1.6×10^5
402249	GaAs	(100)	0.21	1.0μm	50K	6.2×10^{15}	2.0×10^5
1217	GaAs	(100)	0.19	6.2μm	30K	1×10^{16}	2.4×10^5
403250	GaAs	(100)	0.20	1.0μm	40K	1.0×10^{16}	3.0×10^5

II. Doping

N-Type

We have shown in the previous DARPA contract (MDA 903-83K-0251) that indium can be incorporated as an active impurity with a high electrical efficiency in HgCdTe layers during the MBE growth.

Indium is a very good n-type dopant:

(1) it has a high electrical efficiency (70 to 100%) and that without any activation (see fig. 1);
(2) high doping levels up to $10^{19}cm^{-3}$ have been reached;
(3) high electron mobility of $1\times10^{5}cm^{2}V^{-1}s^{-1}$ have been observed for doping level of $2\times10^{16}cm^{-3}$;
(4) abrupt junctions can be grown (see fig. 1).

But indium presents a serious problem. Memory effect has been observed which means that some residual indium (10^{15} - $10^{16}cm^{-3}$ range) is found in epilayers grown after In-doped epilayers have been grown. This effect is supposed to be due to indium-tellurium chemical reaction(s) taking place in different parts of the MBE chamber. The compound(s) can later be reevaporated and dissociated if they are heated. Te, In and CdTe effusion cells have been found to be the sources of contamination along with the walls surrounding the effusion cells and the substrate heater.

This problem has been worked out for months but no satisfactory solution has been found, therefore another n-type dopant has to be investigated.

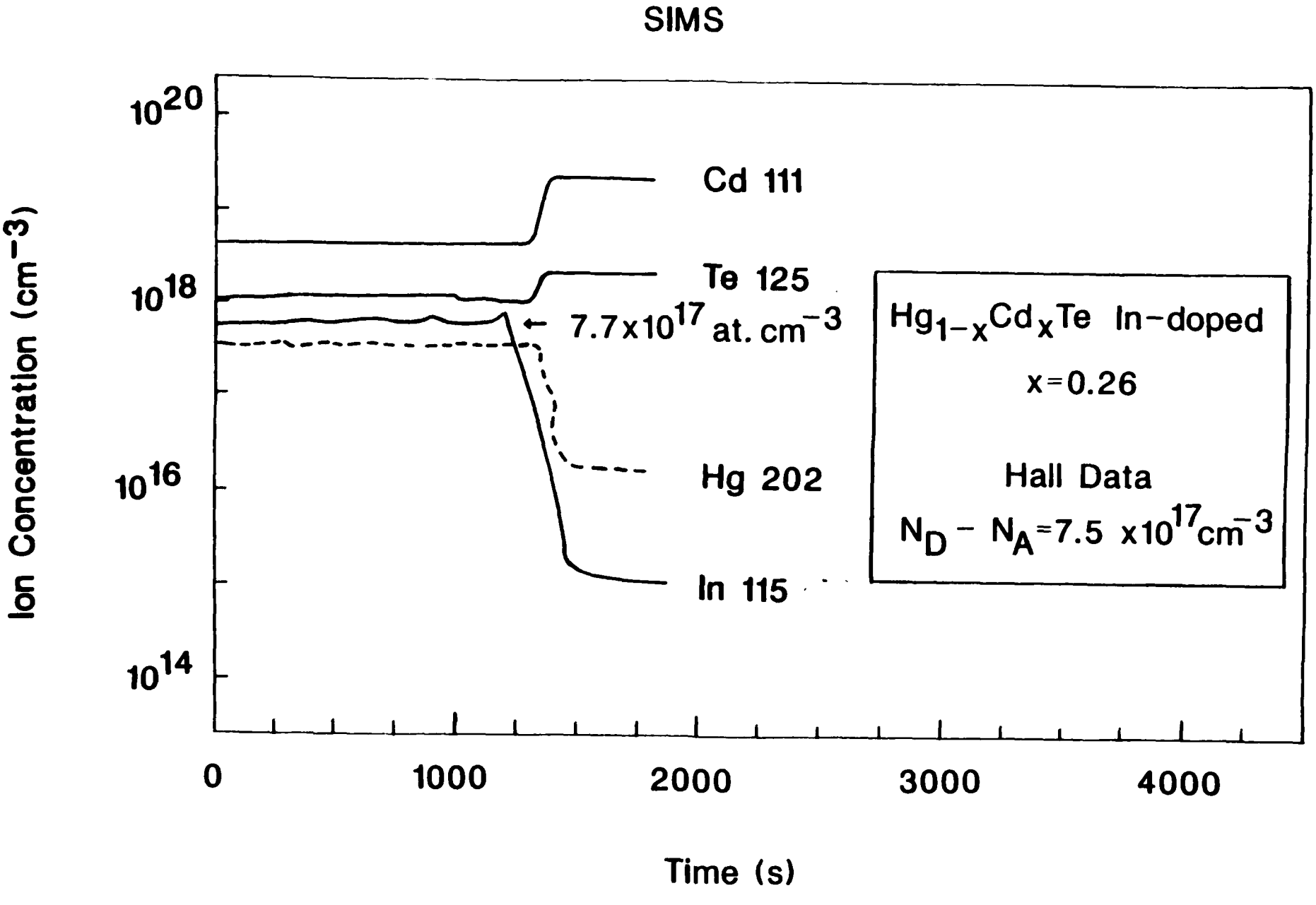
SIMS
Ion Concentration (cm^{-3})
10^{20}
10^{18}
10^{16}
10^{14}
Cd 111
Te 125
7.7×10^{17} at. cm^{-3}
Hg 202
In 115
$Hg_{1-x}Cd_xTe$ In-doped
x=0.26
Hall Data
$N_D - N_A = 7.5 \times 10^{17} cm^{-3}$
0
1000
2000
3000
4000
Time (s)

P-type

Arsenic and Antimony

Group V elements can be incorporated into HgCdTe as acceptors in substitution of non-metal lattice sites using the liquid phase epitaxy. However, group V elements have not been successfully incorporated into MBE grown HgCdTe layer as acceptors. Both Sb and As have been tried and they behave as n-type dopants as illustrated in Table IV and Table V.

A cracker cell has been used for As and Sb which means that the flux was constituted by As_4 + As_2 molecules or by Sb_4 + Sb_2 molecules.

Some of the As doped HgCdTe layers were annealed using the close tube method. For these annealing a drop of Hg was used to control the Hg pressure and the Hg temperature was kept higher than the sample temperature. Table IV shows the electrical measurements of two As doped HgCdTe layers before and after annealing.

The annealing increases the As electrical activity as a donor, and not as an acceptor, by a factor of 4 to 5.

Sample #508331 and 511334 which have been grown with the same As cell temperature have about the same SIMS counts. But sample #511334 has a higher carrier concentration (factor 2 to 3) both before and after annealing. Sample #511334 was exposed to UV light while growing and not sample #508331.

Thus it appears that when exposed to UV light the electrical activity of As in HgCdTe increases as a n-type dopant.

This is not completely surprising if we consider that As is incorporated as a n-type dopant because As-Te bonds are established in preference to As-Hg or As-Cd. UV light is supposed to break Te_2 molecule (E~3eV) making Te even more reactive with As.

These experiments do not conclude that As or Sb cannot be incorporated as p-type dopants in MBE grown layers. SIMS analysis shows that only a few precent of As or Sb are electrically active. In fact, if one considers the heat of formation ΔH_f of some tellurides it appears that ΔH_f for Sb_2Te is equal to -4.5 kcal/mole, less than ΔH_f of HgTe (-7.6 kcal/mole). No data have been found for As_2Te but ΔH_f should not be very different. This means that Sb_2Te and As_2Te are more

unstable than HgTe itself. It is unclear yet how As or Sb are acting as donors incorporated in Hg vacancies or in interstitial sites. But it seems very likely that they could be incorporated as acceptors. A higher Hg flux, light, electron or ion beams have to be investigated.

As-doped HgCdTe ($\overline{111}$)B MBE layers

Sample	x	TAs cell(c)	T_{HALL}(K)	as-grown cc(cm^{-3})	as-grown μ_H($cm^2V^{-1}s^{-1}$)	After annealing cc	After annealing μ_H
133 329	0.22	230	77	n-2.5×10^{16}	7.0×10^3		
8 326	0.22	0	30	p-1.8×10^{16}	600		
508 331	0.28	250	77	n-2.5×10^{15}	5.0×10^3	n-1.5×10^{16}	4.3×10^4
511 334 (UV light)	0.29	250	77	n-8.0×10^{15}	4.5×10^3	n-3.8×10^{16}	2.3×10^4
509 332	0.29	0	30	p-3.0×10^{15}	260		

Sb-doped HgCdTe ($\overline{111}$)B MBE layers

Sample	X	$T_{Sb\ cell}$(c)	Orientation	CC(cm^{-3})	μm($cm^2V^{-1}s^{-1}$)
547 369	0.20	450	(111)	n-8 x 10^{15}	2 x 10^4
551 370	0.20	0	(111)	p-8 x 10^{15}	300
546 368	0.23	350	(111)	n-1 x 10^{15}	1 x 10^4
545 367	0.24	0	(111)	p-2.5 x 10^{16}	600
562 378	0.26	500	(111)	n-2.6 x 10^{15}	9 x 10^3

III. $Hg_{1-x}Cd_xTe/Hg_{1-y}Cd_yTe$ Heterojunctions Grown in Situ by MBE

Insotype n-N abrupt heterojunctions where grown in situ by MBE on CdTe(111)//GaAs(100) combination substrates. The first devices tested had x = .18 on the bottom and x = .26 on the top. All the electrical and optical characterizations were consistent with the presence of narrow and strong composition burst right at the interface. The R_oA was limited by the widegap side (see attached publication entitled "Mercury Cadmium Telluride n-Isotype Heterojunctions Grown in Situ by Molecular Beam Epitaxy."

The later devices grown with care to avoid the problem had drastically different behavior. The compositions where slightly higher on both sides: x = .22 for the bottom and .28 for the top. Strong rectification was seen with quality factors varying from 2 at high temperatures to 2.5 at 80K (fig. 2). The forward bias occurred when the top material was biased negatively. One device had an R_oA as high as 10^4 Ωcm^2 at 80K, but this value was only seen once. In the average it typically reaches 10^3 at 80K (fig. 3). The activation energy of I_s/T^2 varies from .1eV at high temperature to .06eV at 80K (fig. 4). the spectral response shows a maximum at 8μm wavelength, without sharp peak at short wavelength as before (fig. 5). The capacitance measurements are unreliable since the top material thickness was as small as .5μm, and the top contact is suspected to have a smaller area than expected. A low current density $10^{-2}A/cm^2$ can blow the devices opened. These measurements are consistent with a Schottky type behavior at the heterojunction, most of the depletion occurring in the wide bandgap material, which is limiting the R_oA. Thermionic emission is not the only process involved in the transport since the quality factor is higher than 2. This renders the barrier height determination unreliable, even if it seems consistent with the expected bandgap difference between the two sides.

HETEROJUNCTION

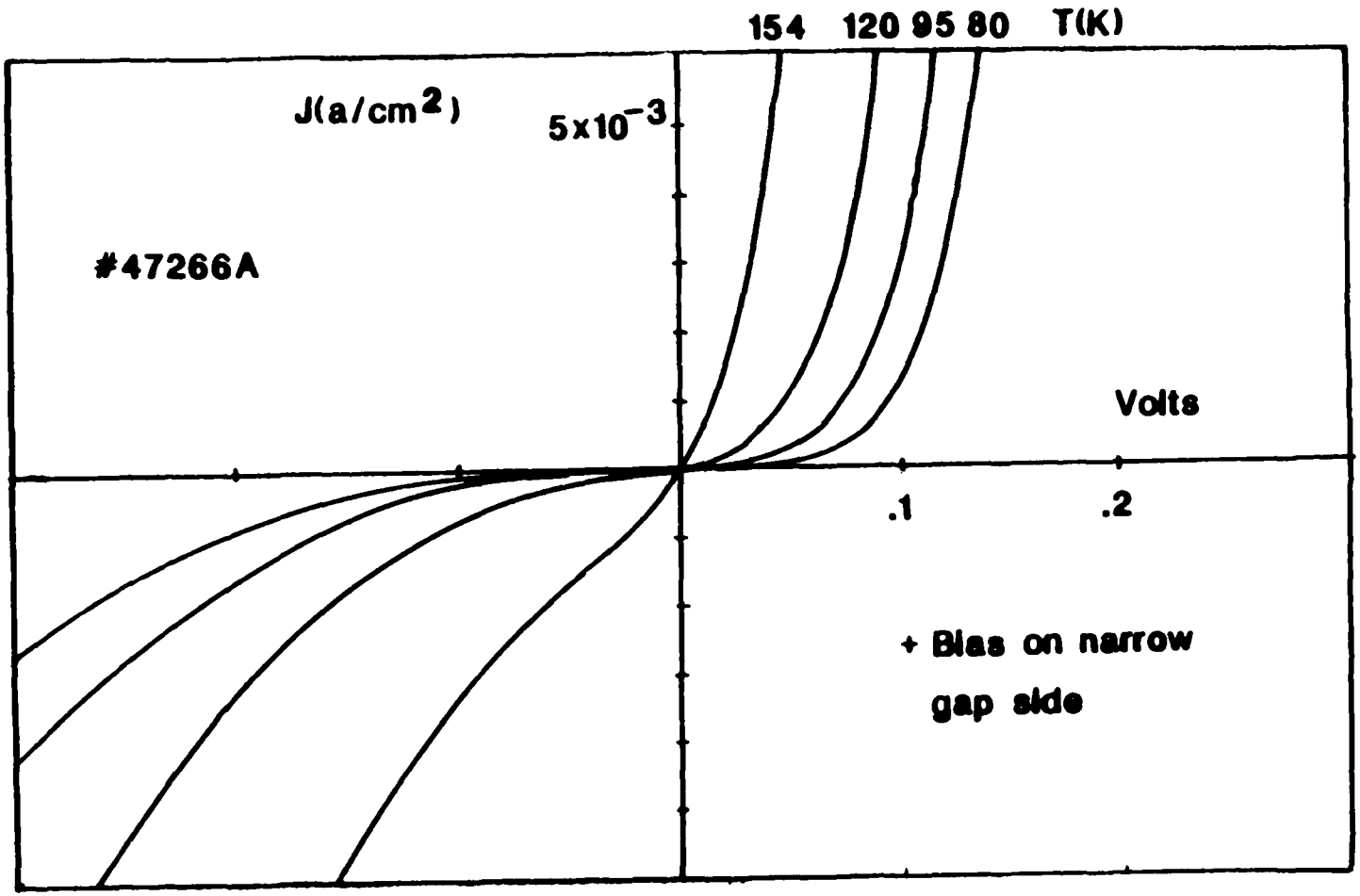

Current Voltage Curves

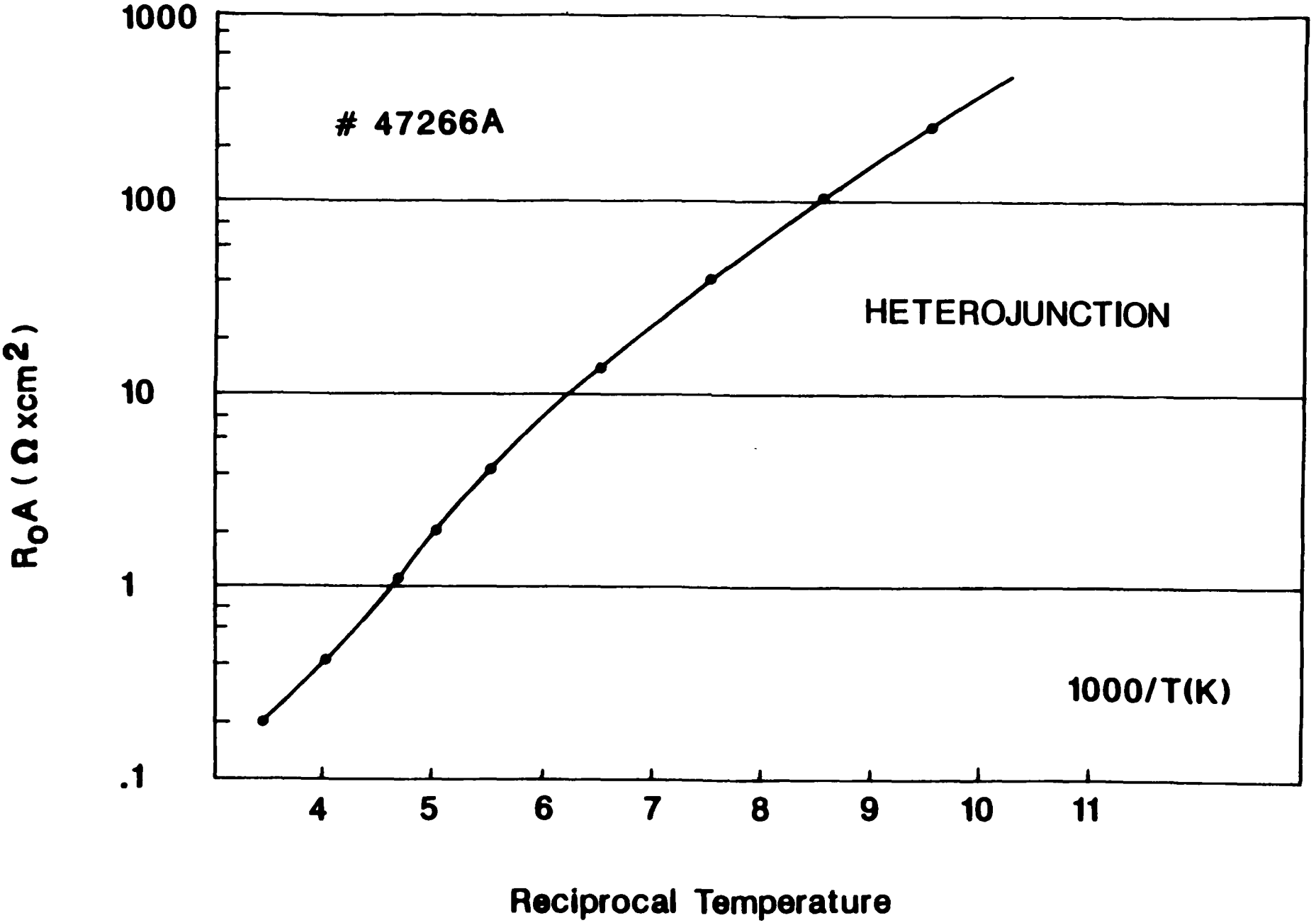
1000
100
10
1
.1
47266A
HETEROJUNCTION
1000/T(K)
R_oA (Ω xcm^2)
4
5
6
7
8
9
10
11
Reciprocal Temperature

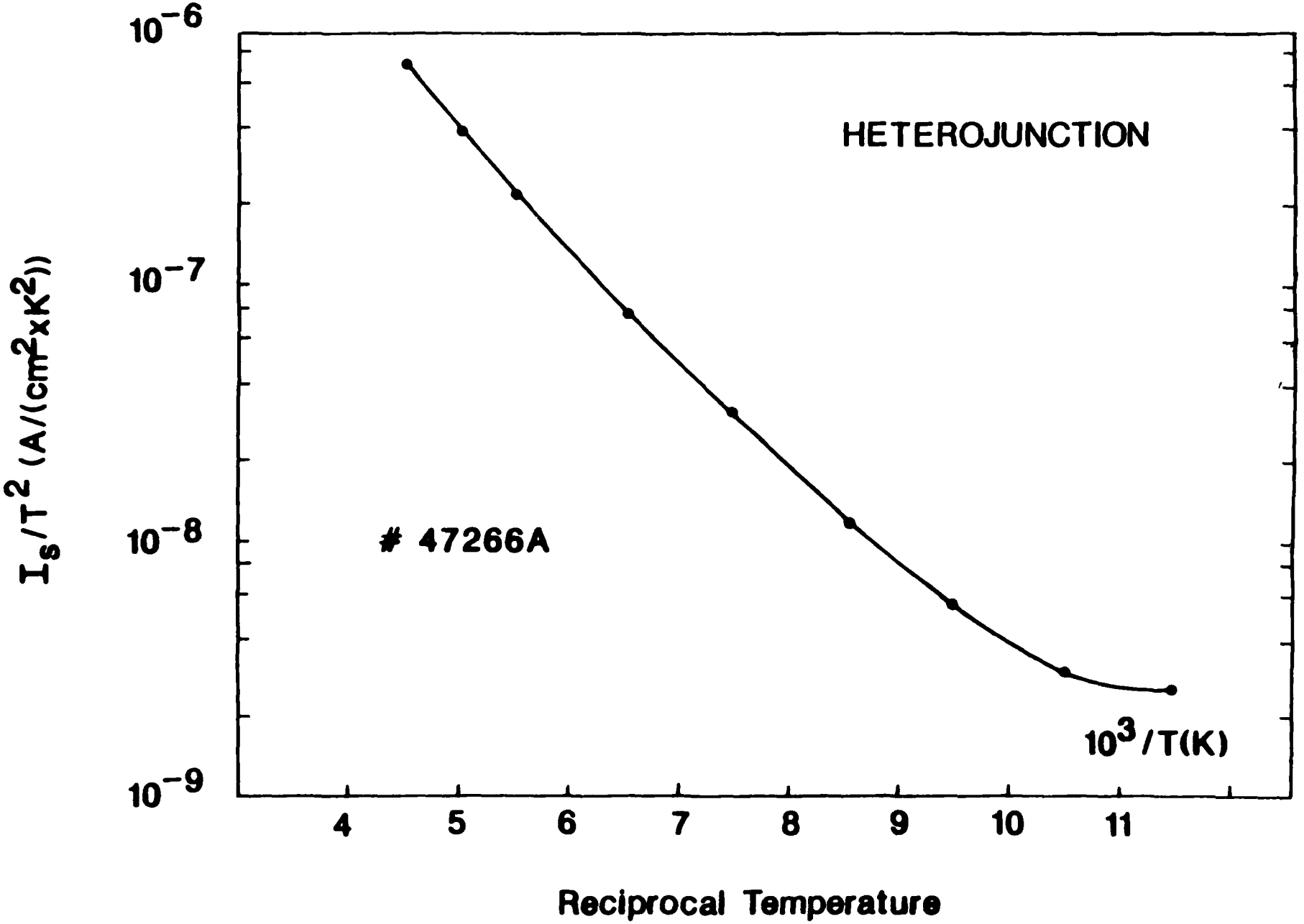
HETEROJUNCTION
47266A
10^{-6}
10^{-7}
10^{-8}
10^{-9}
I_s/T^2 (A/(cm^{2}xK^2))
4
5
6
7
8
9
10
11
10^3/T(K)
Reciprocal Temperature

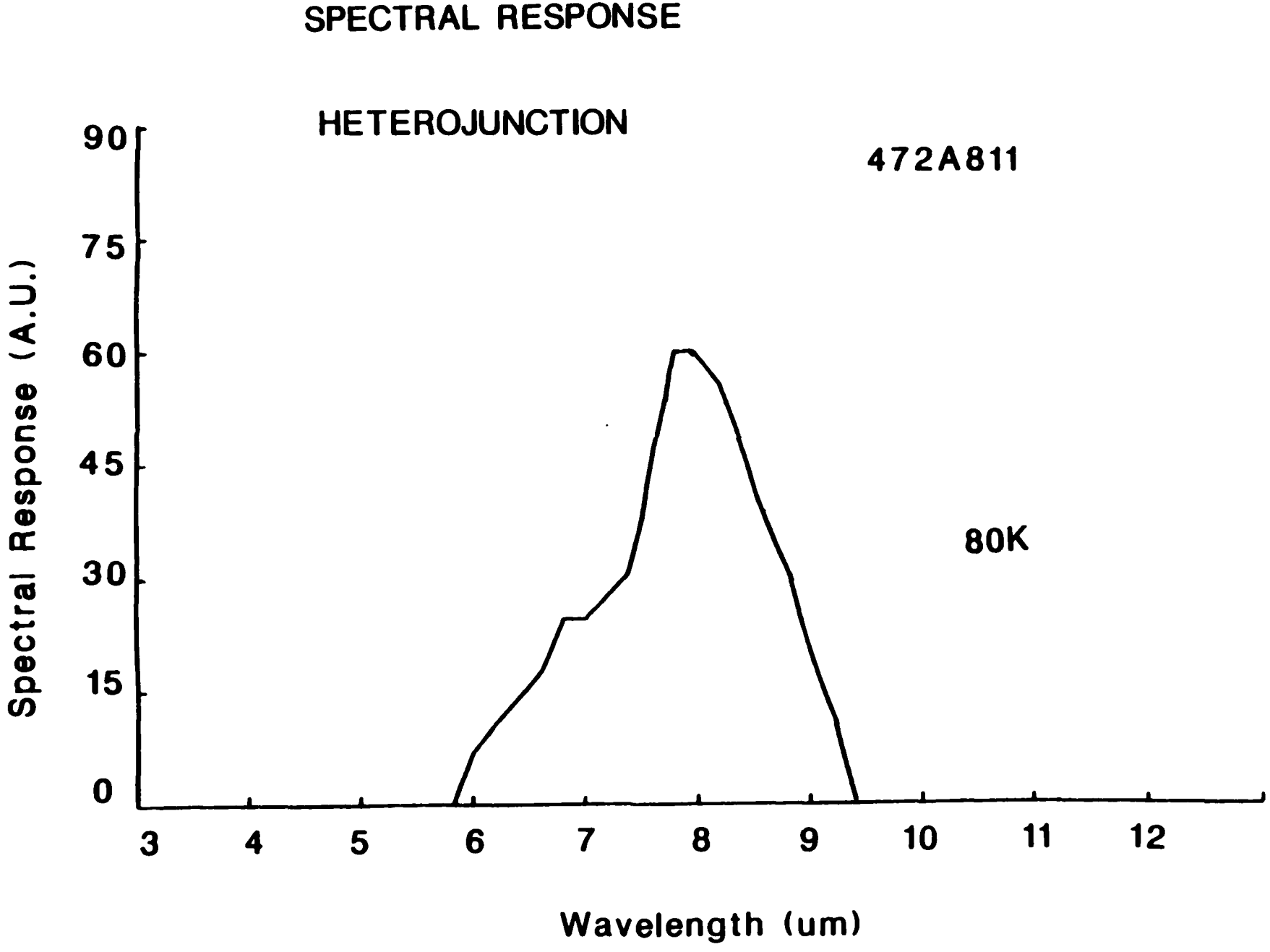
SPECTRAL RESPONSE
HETEROJUNCTION
472A811
80K
Spectral Response (A.U.)
90
75
60
45
30
15
0
3
4
5
6
7
8
9
10
11
12
Wavelength (um)

091705JVA = 091705JVA

Running Title: Mercury cadmium telluride *n*-isotype heterojunctions

Mercury cadmium telluride *n*-isotype heterojunctions grown *in situ* by molecular-beam epitaxy

M. Boukerche, I. K. Sou, M. DeSouza, S. Yoo, and J. Faurie
Department of Physics, University of Illinois at Chicago, Chicago, Illinois 60680

(Received 10 November 1986; accepted 7 May 1987)

Electrical characterizations of the first *n*–*N* HgCdTe heterojunctions grown *in situ* by molecular-beam epitaxy are reported. The cadmium concentrations of the two materials are 0.18 for the bottom layer and 0.26 for the top. The measurements by Hall, *IV*, *CV*, and spectral responsivity are consistent with the existence of a conduction-band barrier at the interface behaving as an insulator at low temperature. We suggest that transient effusion cell fluxes occurring during shutter sequencing created such barriers at the heterojunction interfaces during the growth. The high R_oA (600 $\Omega \times cm^2$) measured suggests that this effect might be of interest for future heterojunction gate field-effect transistor investigations.

I. INTRODUCTION

The $Hg_{1-x}Cd_xTe$ (MCT) ternary alloy is currently the most important material for infrared applications in the 8–12 μm wavelength range. It is also used for the 3–5 μm window and considered for the optoelectronic range. This material can be grown for any cadmium composition x between 0 and 1, and can then be considered as a solid solution. The corresponding forbidden energy gap can be varied continuously between -0.22 and 1.6 eV at 80 K. These unique properties plus the fact that the lattice mismatch between the extreme compositions is only 0.3% make this ternary semiconductor material very attractive for heterojunction investigations. The main motivation for such studies is to improve existing detector performances by tailoring wavelength response, decreasing parasitic currents, and increasing minority-carrier collection efficiencies.

LoVecchio *et al.*[1] studied the case of back-to-back MCT ($x = 0.2$), CdTe heterojunctions. They concluded that a valence-band barrier was present in the devices. *n*/*p* MCT heterojunction photovoltaic devices were demonstrated by Bratt.[2] In certain cases, barrier formation was also reported.

Both groups used the liquid phase epitaxy (LPE) growth technique and reported substantial grading and/or diffusion at the interfaces. Vydyanath *et al.*[3] showed that such effects could actually be profitable since they presented exceptional LPE grown MCT heterojunction detector performances.

The possibility of including semimetallic, semiconducting, and semi-insulating materials within the same monocrystal could lead to important technological applications. The abrupt heterojunctions between these materials have to be further studied.

Kuech and McCaldin[4] reported characterizations of HgTe layers grown by the metalorganic chemical vapor deposition technique at 325–350 °C on *n*-type CdTe. A Schottky barrier behavior was seen, with a maximum barrier height of 0.92eV.

The validity of the common anion rule for the HgTe/CdTe system has been questioned recently.[5] The reported values of the valence-band offset vary from 40 (Ref. 6) to 350 meV[7,8] depending on the technique used. The above workers[1] mention that inversion in the CdTe layer could explain their low barrier height value. We suggest that interdiffusion effects might have played an important role. In any case, most of the band-gap difference should appear in the conduction-band discontinuity.

The molecular-beam epitaxy (MBE) technique is now recognized as a possible choice for the growth of MCT on CdTe and GaAs.[9,10] Its low growth temperature (190 °C) minimizes the interdiffusion effects and allows abrupt interfaces to be produced in thin epitaxial layers like superlattices. Several abrupt *n*-isotype heterojunctions between two narrow-band-gap compositions were grown for the first time in order to observe the transport properties of the electrons through the expected conduction-band discontinuity on the wide-band-gap side. We present here the characterization of mesa devices fabricated from these first samples.

II. EXPERIMENTAL

The junctions were grown on CdTe(111)//GaAs(100) substrates with a Riber 2300 system modified to handle mercury. Both sides of the junction were doped *n* type with indium as previously described.[11] The narrow-gap side was first made with a thickness of 2 to 3 μm before the growth conditions were abruptly changed to produce the wide-gap material up to a thickness of 1.0 μm. The substrate temperature was kept at 190 °C all along the growth. The composition of the narrow gap was determined by infrared transmission measurements at room temperature. Its doping level 4×10^{15} cm^{-3} was deduced from the Hall measurements neglecting the contribution of the wide-gap side. This was relevant since the doping level was intentionally lowered during the growth of the $x = 0.26$ material. The composition and doping ($\sim 5 \times 10^{15}$ cm^{-3}) of the top layer was estimated from the growth conditions on separate runs. To check the doping level, metal–insulator–semiconductor (MIS) structures were fabricated with gold and zinc sulfide on a different piece of the sample. The high-frequency capacitance versus voltage curves were measured at 80 K and 100 kHz with an LCR 4275 from Hewlett-Packard. The classical MIS calculation[12] was used to deduce the impurity level from the minimum to maximum capacitance ratio, where the minimum capacitance was calculated using the approximation of Ref.

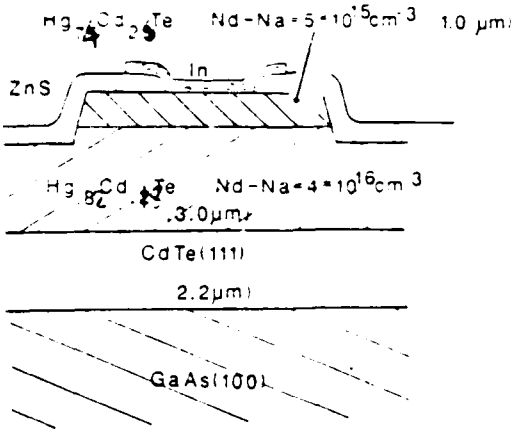

FIG. 1. Structure of the devices

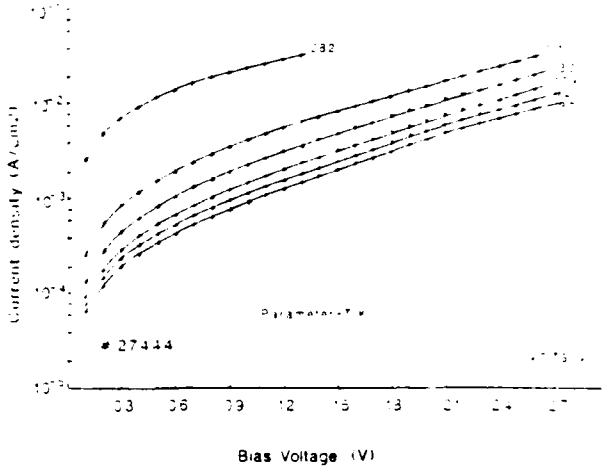

FIG. 3. Semilog plot of the I/V curves when the top material is biased negatively

19. The doping level deduced was within a factor of 2 from the growth esimated value. The devices were made by standard photolitographic techniques and mesa etching. The metal was evaporated over the zinc sulfide passivation opened for contacts. Their structure can be seen in Fig. 1. The geometry is circular to minimize edge leakage but is obviously not optimized for detection applications. The junction area is $7 \cdot 10^{-4}$ cm^2. More than 150 dots were tested from 300 down to 80 K with a microprobe station from MMR Technologies, Inc. The probe connected to the top contact was positioned on the metal part overlaping the zinc sulfide to avoid piezoelectric effects. The current versus voltage measurements were made with an electrometer/voltage source model 617 from Keithley, modified to generate 5-mV steps. All the data acquisition was computerized.

III. RESULTS

The current versus voltage curves measured can be seen in Fig. 2. They are representative of the average of the devices measured. Very weak forward rectification occurs when the top wide-band-gap material is biased negatively. They could be simply described as showing double soft reverse breakdown at low temperature. The current is proportional to the voltage at low bias, and tends to a power of the voltage law (2-3) above 50–100 mV. A semilogarithmic plot of these curves is shown in Fig. 3 for the forward bias case. Notice that their slopes are nearly independent of temperature. The R_0A values could reach 600 Ω cm^2 at 80 K on several devices, showing that the active part of the device is on the wide-band-gap side. Its variation as a function of $1/T$ can be seen in Fig. 4 in reverse bias. At high-temperature it follows an exponential law in a limited range only, and tends to saturate at low temperature. The corresponding high-temperature activation energies are systematically higher in reverse bias (~ 105 meV) than in forward bias (~ 80 meV). The I/V curves were fitted by the least-square method to the equation

$$I = I_0 [\exp(V - IR_s/V_0) - 1], \quad (1)$$

where I is the current density, I_0 the saturated current den-

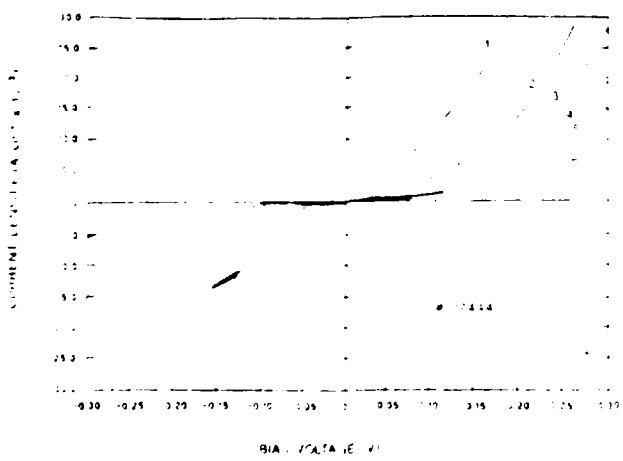

FIG. 2. Current vs voltage curves vs temperature. Positive voltages correspond to negative bias on the top material. Temperatures curve 1: 295 K, 2: 260 K, 3: 232 K, 4: 200 K, 5: 162 K, and 6: 80 K.

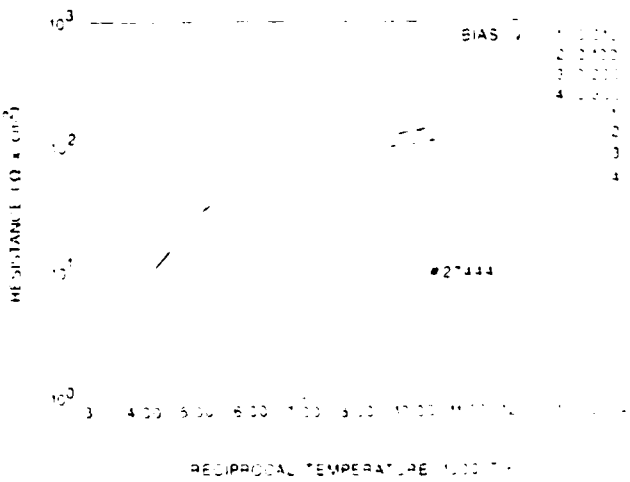

FIG. 4. Variation of the dc resistance of the device with the reciprocal temperature

sity V the bias voltage, R_s the series resistance, and V_0 the voltage defining the slopes of the curves. The precision of the parameters extracted was only questionable close to room temperature where the devices showed an ohmic behavior. Below 150 K, V_0 was found constant and equal to 145 and 80 mV in reverse and forward bias, respectively, and R_s was negligible. V_0 was increasing with temperature above 150 K.

A typical capacitance versus voltage curve is shown in Fig. 5. It clearly does not follow the classical Schottky diode depletion model but rather a metal–insulator–semiconductor device behavior. The frequency dependence is small. The admittance curves correlate the slope variation of the dc current/voltage measurements.

IV. DISCUSSION

The lack of strong rectification implies that thermionic emission is negligible. The current transport is limited by some form of tunneling since it varies as $\exp(V/V_0)$ independently of temperature below 150 K. These properties are systematic for all the devices on several crystals, and are not resulting from a marginal contact process on the top contact which could create back-to-back Schottky diodes randomly. Furthermore, a sharp minimum in capacitance close to zero bias should be seen in this case.[13] Schottky barrier lowering with biasing voltage is not detected since the current should vary as $\exp(\alpha V^{1/4}/T)$,[13] and V_0 should be a function of temperature even at 80 K.

These results have similarities with the theory of thermionic field emission across Schottky barriers (TFS).[14] The ratio kT/E_{00} is an estimation of the relative importance of the thermionic and field emission processes,[15] where k is the Boltzmann constant, T the absolute temperature, and E_{00} an energy defined as

$$E_{00} = (q\hbar/4\pi)(N_D/m^*\epsilon)^{1/2}, \qquad (2)$$

where q is the electronic charge, $\hbar$ Planck's constant, N_D the donor concentration in the semiconductor (in our case the wide-band-gap side with $x = 0.26$), m^* and ϵ the electron effective mass and the static dielectric constant in the same material. When $kT \gg E_{00}$, the current is mainly due to thermionic emission. When $kT \ll E_{00}$, field emission (or tunneling from energies close to the conduction band) is the dominant transport mechanism. Both types of electron emission have to be considered when $kT \simeq E_{00}$. In our case $N_D \simeq 5 \times 10^{15}$ cm^{-3}, and for $x = 0.26$ at $T = 80$ K, the relative electron effective mass and dielectric constant are taken, respectively, as 1.4×10^{-2} and 16.9. The value of E_{00} is then 2.66 meV, much smaller than $kT = 6.9$ meV. The fact that thermionic conduction is not seen in forward bias, together with the capacitance measurements results, make us conclude that a large conduction-band barrier is present at the heterojunction between the two materials. This is in agreement with the spectral response measured on one device in small reverse bias at 80 K, showing a wide response in the 3–6 μm range and a peak more than three times higher in amplitude at 1.9-μm wavelength. The root square of the photoresponse is shown versus wavelength in Fig. 6. The low-energy tail was close to the noise floor and was separated from the response of the $x = 0.26$ material by more than 1 μm. The measurement was made under vacuum with a glow bar infrared source, a monochromator, and a lock-in amplifier. The curve was corrected for blackbody radiation and grating dispersion. It can be interpreted as internal photoemission from a conduction-band barrier 0.56 eV above the Fermi level (being degenerate in the narrow-band-gap material). The TFS theory predicts that the current/voltage relation should be of the form[14]

$$I = I_0 \exp(qV/E_{00}) \qquad (3)$$

at high enough voltages, where $E_{00} = E_{00}\coth(E_{00}/kT)$ and I_0 is a function of T, the barrier height, the doping level, and is a weak function of the bias. E_{00} has been previously introduced.

Since $E_{00} = 80$ meV below 150 K in our devices, we can see that the rise in E_{00} above this temperature cannot be accounted for by the TFS theory. Tunneling through a high and

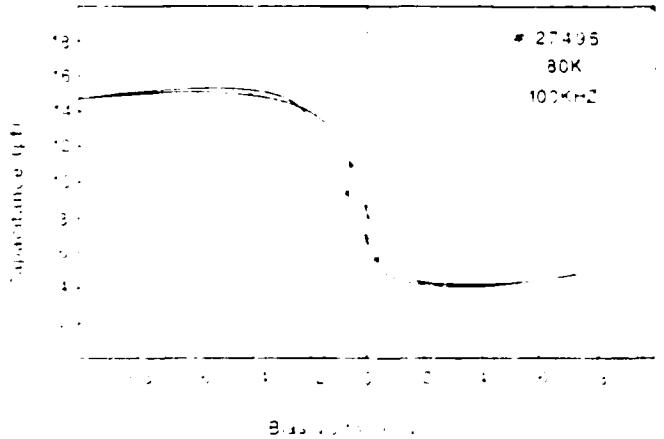

Fig. 5. [illegible] capacitance versus voltage curves at low temperatures. Positive voltages correspond to positive bias on the top material.

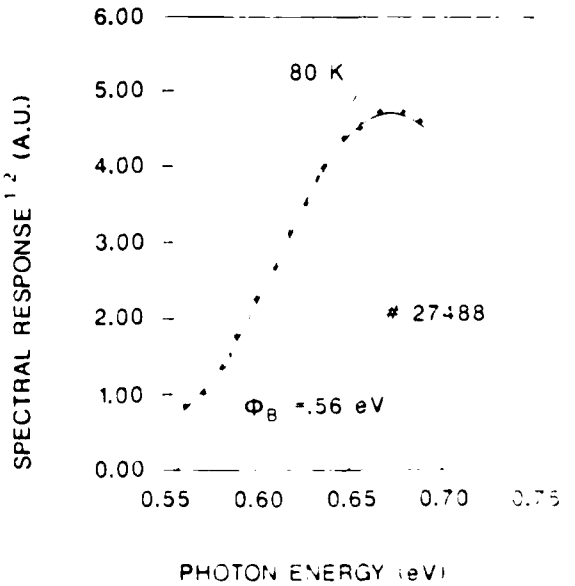

Fig. 6. Root square of the spectral response of the device as plotted versus the high-energy tail is shown.

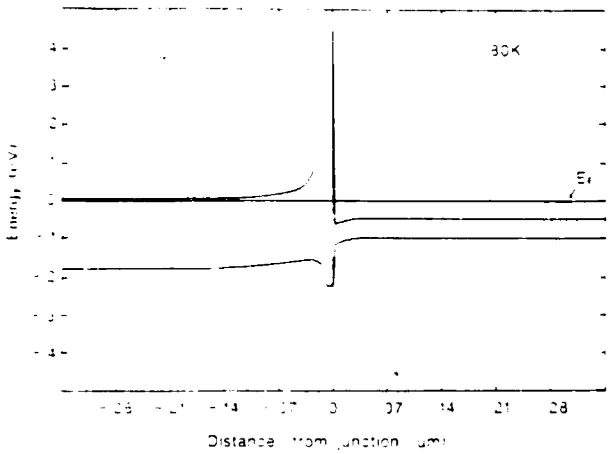

FIG. 7. Calculation of the assumed band profile of the structure at zero bias. Parameters used: $m^*_{hh}/m = 0.44$, doping left-hand side $= 5 \times 10^{15}$ cm^{-3}, doping right-hand side $= 4 \times 10^{16}$ cm^{-3}, Cd composition left-hand side $= 0.26$, Cd composition right-hand side $= 0.18$, Cd composition at the barrier peak $= 0.6$, $\Delta E_v = 0.15 \times \Delta E_g$, $T = 80$ K.

sharp barrier is the suspected dominant transport at low T. Only a minor contribution to the current is due to band bending change with bias in the $x = 0.26$ material. As will be discussed later, we think that the barrier resulted from abrupt composition change during growth. Its actual conduction-band profile is expected to be much steeper than the parabolic potential approximation made in the TFS theory.

A Poisson solution of the expected band profile of the device at 80 K is shown in Fig. 7. An abrupt Cd composition increase up to $x = 0.6$ was assumed right at the interface, followed by a sharp exponential decrease down to $x = 0.26$. The minimum barrier thickness was set to be 100 Å. The valence-band offset between two different composition materials was assumed to be 15% of their band-gap difference. A heavy-hole effective mass independent of composition and equal to 0.44 has been used. The calculation is made with the relaxation method, using the two-band Kane[16] model and assuming fully ionized dopants without diffusion effects at the interface. Degeneracy is included. The details of this calculation will be presented elsewhere.[17] We can see that the Fermi level on the left-hand side is within 1 meV of the conduction band, whereas the narrow bandgap is heavily degenerate, the Fermi level lying 45 meV above the conduction band.

This structure basically looks like a metal–insulator–semiconductor device as suspected from the capacitance measurements. The semiconductor with $x = 0.26$ is weakly degenerate. The use of a metal–insulator–metal tunneling model could be appropriate at low temperature where we established that tunneling transport is dominant. We used the model developed by Simmons[18] for its simplicity, modifying it slightly to make provision for different effective masses in the metal and the insulator. It assumes a rectangular barrier and is restricted to low temperatures where the tunneling is independent of temperature. We did not use it in the first place since it cannot demonstrate the existence of the tunneling process by itself. The current density is given by

$$I = (1/R_0)\{(\Phi_B - V/2)\exp(-A\sqrt{\Phi_B - V/2}) - (\Phi_B + V/2)\exp(-A\sqrt{\Phi_B + V/2})\}$$

with $A = 4\Pi d\sqrt{2m_i q}/h$,

$$R_0 = (2\Pi h d^2/q^2)(m_i/m_m),$$

where d is the thickness of the barrier, Φ_B the barrier height, V the bias, h Planck's constant, and q the electronic charge. m^*_i and m_m are the electron effective masses in the insulator and the metal electrode acting as the cathode, respectively. R_0 is not to be confused with the zero bias resistance of the device.

The effect of barrier height lowering is not considered since it could not be detected from the measurements and the barrier height is expected to be large. The fact that the curves in Fig. 3 are nearly symmetric is consistent with this model. The low-temperature curve of Fig. 3 was fitted in reverse bias since the tunneling is less affected then in forward bias by the actual barrier profile on the wide-band-gap side. Φ_B and d where adjusted to produce the results shown in Fig. 8. The following effective masses have been used: $m_i/m_0 = 0.058$ and $m^*_m/m_0 = 0.0039$. It can be seen that the best fit occurs for $\Phi_B = 0.55$ eV, in excellent agreement with the optical result. The average matching barrier thickness is close to 110 Å.

The capacitance measurements can be interpreted as follows: the diode is essentially behaving as an MIS where the narrow-band-gap material is the metal electrode and the barrier is the insulator. The top semiconductor with $x = 0.26$ is then seen n-type in depletion at zero bias. Calculation of the low-frequency differential capacitance of the structure shown in Fig. 7 was attempted using the same type of calcu-

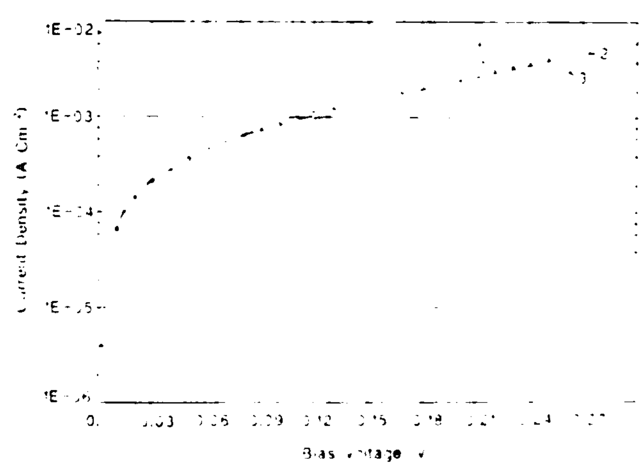

FIG. 8. [illegible] Parameters used:

	Φ_B (eV)	d (Å)
Curve 1	0.45	[illegible]
Curve 2	0.55	[illegible]
Curve 3	0.65	[illegible]

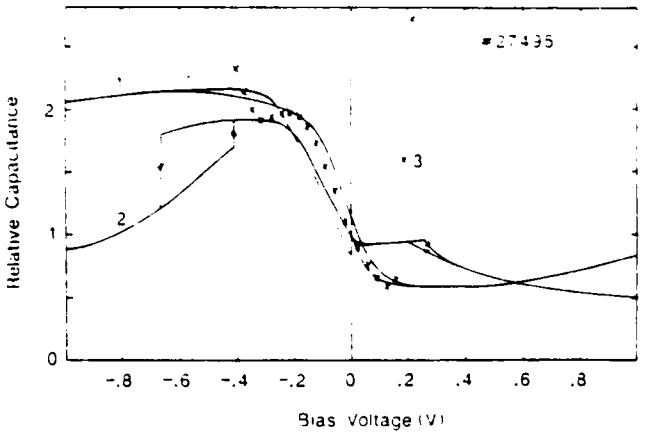

FIG. 9. Relative capacitance vs voltage curves. Curve 1: second measurement of the CV data shown in Fig. 5 ($T = 80$ K, 100 kHz). Curve 2: measurement of the same device with the same frequency ($T = 160$ K). Curve 3: Low-frequency capacitance calculation at 80 K. Same parameters as in Fig. 7.

lation as before and the same parameters. The quasi-Fermi levels on each side of the heterojunction were assumed to be constant, their difference being abruptly accommodated at the interface. The result is shown in Fig. 9, together with measurements made at 80 and 160 K at 100 kHz on the same device. We can see that an accumulation plateau occurs below -0.2 V. Its magnitude is much smaller than the capacitance of the pseudoinsulator alone. This is due to the onset of depletion on the narrow-band-gap side which begins to be inverted below -0.3 V. The high-frequency low-temperature CV curve then stays approximately constant thereon. The calculation also shows strong inversion of the wide-band-gap side to be occurring at -0.15 V. Notice that these thresholds tend to precede the abrupt falls in capacitance measured at 160 K. We think that these transitions are linked to the collapse of their corresponding hole inversion layers through the valence side of the burst barrier, driving their respective material side in deep depletion. It demonstrates that hole confinement against this barrier occurred before. We conclude that a valence-band barrier is also present, and that the valence-band offset cannot be neglected. Even though no precise value can be deduced from this work, we should point out that the 15% of the band-gap difference value used in the calculations is consistent with all the measurements made as well as the recently published studies[7] when extrapolated to the HgTe/CdTe case. At the present time the reason why the capacitance only collapses at high temperatures is not clearly understood. It might be linked to two-dimensional quantized energy levels of the inversion layers interacting with deep levels within the bursting material. Even though the deep levels have been omitted from this study, they are known to be present since noticeable hysteresis has been seen in the CV measurements, and to a smaller degree in the IV measurements. They could also contribute to the enhanced tunneling process described.

The burst in composition which occurred at the interface is linked to the transient flux response of the effusion cell opened during the growth to increase the cadmium content of the top layer. When the shutter is closed, the cell has a higher quasiequilibrium pressure than with the shutter opened. This study shows that with the particular geometry used the time constant required by the cell to change from the closed to opened stable conditions was in the order 15 s. Once detected, this problem can be avoided. Recently grown devices trying to avoid this effect give credit to this hypothesis and will be published later.

V. CONCLUSION

We showed that the electrical characterizations of the first abrupt *n*-isotype heterojunctions made by MBE were consistent with the presence of a sharp burst in composition at the heterojunction interface due to the growth conditions.

The measurements and the calculations presented are in agreement with the presence of a valence-band offset between the barrier material and the adjacent layers. When extrapolated linearly to the HgTe/CdTe case, the value assumed is in agreement with the recently published studies. The high R_oA values obtained even for a narrow-gap composition $x = 0.17$ could be of interest for future gate field-effect transistor investigation.

ACKNOWLEDGMENTS

This work was funded by DARPA Contract No. MDA903-85K-0030. One of us (M. E. D.) has also a scholarship from CNPq-Brazil.

[1] P. LoVecchio, M. B. Reine, and M. N. Grimbergen, J. Vac. Sci. Technol. A **3**, 246 (1985).
[2] P. R. Bratt, J. Vac. Sci. Technol. A **1**, 1687 (1983).
[3] H. R. Vydyanath, S. R. Hampton, P. B. Ward, L. Fishman, J. Stasiewski, and T. Krueger, 1986 IRS Detector Specialty Group Meeting, NASA AMES Research Center, Moffet Field, CA.
[4] T. F. Kuech and J. O. McCaldin, J. Appl. Phys. **53**, 3121 (1982).
[5] J. Tersoff, Phys. Rev. Lett. **56**, 2755 (1986).
[6] Y. Guldner, G. Bastard, J. P. Vieren, M. Voos, J. P. Faurie, and A. Million, Phys. Rev. Lett. **51**, 907 (1983).
[7] S. P. Kowalczyk, J. T. Cheung, E. A. Kraut, and R. W. Grant, Phys. Rev. Lett. **56**, 1605 (1986).
[8] T. M. Duc, C. Hsu, and J. P. Faurie, Phys. Rev. Lett. **58**, 1127 (1987).
[9] J. P. Faurie, A. Million, R. Boch, and J. L. Tissot, J. Vac. Sci. Technol. A **1**, 1593 (1983).
[10] J. P. Faurie, S. Sivananthan, M. Boukerche, and J. Reno, Appl. Phys. Lett. **45**, 1307 (1984).
[11] M. Boukerche, J. Reno, I. K. Sou, C. Hsu, and J. P. Faurie, Appl. Phys. Lett. **48**, 1733 (1986).
[12] S. M. Sze, *Physics of Semiconductor Devices*, 2nd ed. (Wiley, New York, 1981).
[13] C. N. Van Opdorp, thesis, Technical University Eindhoven (1977).
[14] F. A. Padovani and R. Stratton, Solid State Electron. **9**, 695 (1966).
[15] C. R. Crowell and V. L. Rideout, Solid State Electron. **12**, 89 (1969).
[16] E. O. Kane, J. Phys. Chem. Solids **1**, 249 (1957).
[17] M. Boukerche and J. P. Faurie, Solid State Electron. (submitted).
[18] J. G. Simmons, J. Appl. Phys. **34**, 1793 (1963).
[19] E. H. Nicollian and J. R. Brews, *MOS (Metal Oxide Semiconductor) Physics and Technology* (Wiley, New York, 1982), p. 764.

END

FEB.

1988

DTIC